Revision 2

A spectroscopic and carbon-isotope study of mixed-habit diamonds: Impurity characteristics and growth environment

D. Howell[1*], W.L. Griffin[1], S. Piazolo[1], J.M. Say[2], R.A. Stern[3], T. Stachel[3], L. Nasdala[4], J.R. Rabeau[2], N.J. Pearson[1], S.Y. O'Reilly[1]

[1] ARC Center of Excellence for Core to Crust Fluid Systems (CCFS) and GEMOC, Department of Earth & Planetary Science, Macquarie University, NSW 2109, Australia

[2] ARC Center of Excellence for Engineered Quantum Systems (EQUS), Department of Physics and Astronomy, Macquarie University, NSW 2109, Australia

[3] Canadian Center for Isotopic Microanalysis, Department of Earth and Atmospheric Sciences, University of Alberta, Edmonton, AB, T6G 2E3, Canada

[4] Institut für Mineralogie und Kristallographie, Universität Wien, Althanstraße 14, 1090 Vienna, Austria

(e) daniel.howell@mq.edu.au

ABSTRACT

Mixed-habit diamonds have experienced periods of growth where they were bounded by two surface forms at the same time. Such diamonds are relatively rare and therefore under-investigated. Under certain physical and chemical conditions, smooth octahedral faces grow concurrently with rough, hummocky cuboid faces. However, the specific conditions that cause this type of growth are unknown. Here we present a large array of spectroscopic data in an attempt to investigate the impurity and carbon-isotope characteristics, as well as growth conditions, of thirteen large (>6 mm diameter) plates cut from mixed-habit diamonds. The diamonds all generally have

high nitrogen concentrations (>1400 ppm), with the octahedral sectors enriched by 127 – 143 % compared to their contemporary cuboid sectors. Levels of nitrogen aggregation are generally low (2 – 23% IaB) with no significant difference between sectors. IR-active hydrogen features are predominantly found in the cuboid sectors with only very small bands in the octahedral sectors. Platelet characteristics are variable; only one sample shows a large B′ band intensity in the octahedral sector, with no platelets occurring in the cuboid sector. Other samples either show a small B′ band in both sectors, or just in the cuboid sector, or none at all. These data support a model that shows the concentration-adjusted aggregation rate of nitrogen to be the same in both sectors, whereas the subsequent platelet development is reduced in the cuboid sectors. This is because the interstitial carbon atoms have interacted with *disc-crack-like* defects only found in cuboid sectors, which in turn reduces their chances of aggregating to form platelets. These *disc-crack-like* defects are also thought to be the most likely site for the IR-active hydrogen features and they maybe intrinsic to cuboid growth in mixed-habit diamonds. When they are graphitized, as they are in all of the diamonds in this study, this may reflect a heating event prior to volcanic exhumation. Spectroscopic analysis of the green cathodoluminescence exhibited by all of the diamonds shows nickel centers to be present in only the cuboid sectors. Carbon isotope data, obtained by secondary ion mass spectrometry, show very little variation in seven of the diamonds. The total range of 217 analyses is -7.94 to -9.61 (±0.15) ‰, and the largest variation in a single stone is 0.98 ‰. No fractionation in carbon isotopes is seen between octahedral and cuboid sectors at the same growth horizon. These data suggest that the source fluid chemistry, as well as pressure, temperature and oxygen fugacity were very stable over time, allowing such large volumes of mixed-habit growth to occur. The high concentration of impurities, namely nitrogen

and hydrogen, is probably the critical factor required to cause mixed-habit growth. The impurity and isotopic data fall in line with previous modeling based on diamond growth from reduced carbonates with the loss of a ^{13}C-enriched CO_2 component.

Keywords: Mixed-habit diamonds, FTIR mapping, nitrogen concentration and aggregation states, carbon isotopes, nickel defects.

INTRODUCTION

Diamonds are direct samples from the deep lithosphere, the transition zone and the lower mantle (Stachel, 2001). The lattice-bound impurities within them, the mineral and fluid inclusions they encapsulate, and their growth history all provide information on the fluid-related processes occurring at these depths (see review by Stachel & Harris (2008) and references therein). The type of crystal growth that occurs, and the resultant diamond morphology, are dependent on five key factors (Sunagawa, 1990; 2005); (1) the supercritical fluid, (2) the solute-solvent interaction energies (i.e. redox reactions), (3) the degree of carbon saturation, (4) the impurities present, and (5) the pressure (P) and temperature (T) conditions. As a result, detailed knowledge of the characteristics of the different growth types allows us to use diamonds as recorders of mantle conditions and their evolution.

Diamonds commonly only exhibit one growth mechanism at a time. For example, coated diamonds represent two distinct growth periods, with a young opaque fibrous coat forming on an older transparent octahedral core (e.g. Boyd et al., 1992; Tomlinson et al., 2006; Araujo et al., 2009; Weiss et al., 2009). Other diamonds

show transitions between different growth mechanisms (e.g. fibrous to octahedral (Rondeau et al., 2004; Skuzovatov et al., 2011) or octahedral to cuboid to fibrous (Howell et al., 2012a)), suggesting more gradational changes in the environmental conditions. In contrast, mixed-habit diamonds are rare examples of crystals that exhibit periods of growth where they were bound by two surface forms; (1) smooth, flat {111} facets termed octahedral growth and (2) hummocky, non-faceted surfaces, whose mean orientation is {100}. This mixed-habit growth was first recognized by Frank (1967), following a series of etching experiments that revealed curved growth forms (Harrison & Tolansky, 1964; Seal, 1965). Lang and co-workers (Moore & Lang, 1972; Lang 1974; Suzuki & Lang, 1976a, b) termed these curved surfaces "cuboid"; however, they can be inclined by up to 30^{o} off true {100} orientations and where two cuboid faces meet they can create a V-shaped valley. This type of growth can result in a center-cross or star-shaped pattern forming within the diamond (e.g. Welbourn et al., 1989; **Fig. 1**). This cross feature is the result of light-scattering defects being present in the cuboid growth sectors but absent in the octahedral sectors (Lang, 1974). These have been shown to be circular *disc-crack-like* defects on the {111} planes (Walmsley et al., 1987), and they can be either transparent or opaque. It remains unknown whether these defects are intrinsic to cuboid diamond growth.

Most of the early studies on mixed-habit diamonds by Lang and co-workers (for references see above) used X-ray topographs to reveal internal structure. This type of analysis led to conclusions regarding impurity distributions based upon the "spike" X-ray reflection, which related to the formation of platelets - interstitial carbon aggregates that are by-products of the nitrogen aggregation process (see Discussion). This platelet X-ray feature was significantly stronger in the octahedral sectors than in the cuboid sectors and thus Lang and colleagues concluded that

103 octahedral sectors were enriched in nitrogen compared to contemporary cuboid
104 sectors. An infrared (IR) and photoluminescence (PL) spectroscopy study by
105 Welbourn et al. (1989) of numerous cube-shaped diamonds from the Jwaneng mine
106 (Botswana) confirmed the enrichment of nitrogen in octahedral sectors. However,
107 they showed that there was no clear difference in the amount of nitrogen aggregation
108 and subsequent platelet formation between the sectors. They also noted a correlation
109 between strong hydrogen-related absorption bands and the "cloud-like" defects
110 present in the cuboid sectors. The study also attributed the characteristic yellow-green
111 cathodoluminescence (CL) to the S1 and S3 (nickel-related) defect centers.
112 Later studies of mixed-habit diamonds have only provided limited carbon-
113 isotope (Bulanova et al., 2002; Cartigny et al., 2003; Zedgenizov & Harte, 2004;
114 Howell et al., 2012b) and spectroscopic data (luminescence, ultraviolet (UV) and IR
115 absorption, and Raman; Rondeau et al., 2004; Lang et al., 2004; 2007). The results of
116 these studies are briefly summarized here. In contrast to what has been observed in
117 synthetic diamonds (Boyd et al., 1988; Reutsky et al., 2008), there is no fractionation
118 of carbon or nitrogen isotopes between contemporary octahedral and cuboid sectors.
119 Hydrogen-related absorption features are significantly stronger in the cuboid sectors.
120 Nitrogen concentrations are always high (900 – 2500 ppm), with the octahedral
121 sectors always more enriched (107 – 157 % with respect to the cuboid sectors). While
122 nitrogen aggregation levels vary from 0 – 100 % IaB, there remains no unanimity in
123 the literature as to whether there is any significant difference between sectors. This
124 uncertainty propagates into the available data regarding platelet distribution; the B′
125 feature is commonly reported as being much weaker or completely absent in the
126 cuboid sectors, when compared to platelet-bearing octahedral sectors.

Rondeau et al. (2004) presented the first hypothesis regarding the conditions that may produce mixed-habit diamonds. Their principle conclusion was that the large hydrogen features observed in the infrared spectra of only the cuboid sectors meant that high hydrogen concentrations in the source fluid were required for cuboid growth to occur. More recently, Howell et al. (2012b) added to this proposal by incorporating the crystal growth theory of Sunagawa (1990; 2005). When a diamond crystal is bounded by both rough {100} and smooth {111} growth (as is the case for mixed-habit diamonds), the redox reactions and/or impurities present (see Introduction) slow down the growth rate of the rough face, stopping it from being grown out of the crystal, and allowing it to develop as a large habit-controlling face.

In this study, we combine data from several spectroscopic and geochemical techniques with crystal orientation data on a suite of thirteen mixed-habit diamonds, to identify the specific growth environment that may create this special type of diamond crystal. We used IR absorption mapping to study the distribution of nitrogen, hydrogen and platelet related defects, as well as to investigate the presence of any mineral or fluid phases. Raman spectroscopy was used to investigate the dark defects within the cuboid sectors, while photoluminescence was applied to investigate the cause of the green cathodoluminescence observed in the cuboid sectors. Finally, secondary-ion mass spectrometry provided carbon-isotope data to gain chemical insights into the source of the diamond-forming fluids.

SAMPLES

The thirteen diamond samples (MC01 - MC13; **Fig. 2**) exhibited varying proportions of mixed-habit growth. The samples were obtained from the gem trade in

the form of parallel-polished plates; their geographical source is unknown. They range in size from 6 to 13 mm (longest axis), all being less than 1 mm thick.

ANALYTICAL TECHNIQUES

To distinguish between different growth sectors and stages, detailed black and white cathodoluminescence (CL) images were collected for all the diamonds on a Zeiss EVO 15 scanning electron microscope (SEM; GAU, Macquarie University). Accelerating voltages were varied between 15 and 25 kV to obtain the best quality of images. The sample was cleaned and carbon-coated prior to imaging. To confirm the color of the CL, the samples were also examined using a CCL 8200 mk4 luminoscope (10 – 15 kv and 400 – 500 nA) coupled to a Nikon Eclipse ME600 microscope. In addition, optical-light micrographs were obtained on a Leica MZ FLIII microscope using a Leica DFC 500 camera.

Electron backscatter diffraction (EBSD) was carried out on all 13 samples to confirm their crystallographic orientation. The analysis was carried out on a Zeiss Ultra Plus (University of Sydney). Working conditions during acquisition of EBSD patterns were 20 – 25 kV accelerating voltage, ~ 0.8 nA beam current, working distance of about 20 mm, 70° sample tilt, and high vacuum mode (samples carbon coated). Patterns were acquired on rectangular grids by moving the electron beam at a regular step size of 0.1, 1 and 2 μm. EBSD patterns were indexed using CHANNEL 5 software from HKL Technology - Oxford Instruments. The EBSD patterns from the diamond were automatically indexed by comparing obtained reflector intensities with those of theoretical reflectors. For this procedure, we compared to 50 theoretically-calculated reflectors.

To obtain data on the most common impurities found in diamond, Fourier-transform IR spectroscopy was performed using a Nicolet iN10 microscope (GAU, Macquarie University), operated via Omnic Picta software. Using a 100 × 100 μm aperture and a liquid nitrogen-cooled detector, each spectrum was collected over the range of 4000 – 675 cm^{-1} with a resolution of 1 cm^{-1}, by 16 scans in 6 seconds. IR maps were compiled for each sample by recording spectra at 100 μm intervals so that full coverage was obtained. Each map contains between 2933 – 8413 spectra. The spectra were automatically deconvoluted using the DiaMap freeware (see Howell et al., 2012a for a full description of the different components used to calculate nitrogen concentrations and aggregation states). However, where the high nitrogen concentrations cause saturation in the one-phonon region of the spectra, the automated processing technique results in unacceptable errors in the nitrogen measurements. Therefore, only the hydrogen-related data (3107 cm^{-1} band intensity) are presented as maps in this study. Where possible, individual analyses were also recorded at the positions of the SIMS analysis (see below) using a 60 × 60 μm aperture and 64 scans (**Supplementary data**).

To obtain quantitative nitrogen impurity data, individual spectra were extracted from the IR maps and deconvoluted using the same methodology as DiaMap but with one important modification. To prevent the effect of the saturated spectra on the least-squares fitting approach, a saturation level is set prior to the deconvolution. This is a value (in absorption coefficient, cm^{-1}) above which the data from the fit to the spectrum are omitted from the 'sum of the squares' (**Fig. 3**), but the contributions from the different nitrogen components to the overall concentration are retained. When the saturation is mostly in the region of the main A center feature (i.e. ~1260 – 1310 cm^{-1}; Boyd et al., 1994) the uncertainty is thought to be only slightly worse than

the 10% that has been estimated for the normal deconvolution technique. However, when there is additional saturation in the region of the main B center feature (i.e. ~1180 – 1220 cm^{-1}; Boyd et al., 1995) it is thought that this process will underestimate the B center component; therefore the uncertainty is thought to be closer to 20%.

High-resolution Raman spectra were obtained to identify the dark light-scattering bodies only observed in the cuboid sectors, using a dispersive Horiba LabRAM–HR800 spectrometer (Institute of Mineralogy and Crystallography, University of Vienna). The system was equipped with an Olympus BX41 optical microscope, a diffraction grating with 1800 grooves/mm in the optical beam path, and a Si-based, Peltier-cooled charge-coupled device (CCD) detector. Spectra were obtained from the dark bodies inside the cuboid sectors using the 532 nm emission line of a He-Ne laser (≈8 mW at the sample surface). The system was operated in the confocal mode, with the confocal aperture set to 100 μm, and a high-magnification objective (Olympus 100×; numerical aperture 0.90) was used. The resulting spatial resolution varied appreciably with the surface quality of the diamond and the focal depth below the surface; the lateral resolution is estimated at 2 – 3 μm. The system was calibrated using Ne lamp emissions and the Rayleigh line; the wavenumber accuracy was better than 0.5 cm^{-1}. The spectral resolution was determined to be 0.8 cm^{-1}.

The photoluminescence (PL) spectra were collected in order to identify the defects responsible for the strong luminescence, using a room-temperature home-built sample-scanning confocal microscope as previously described by Bradac et al. (2009). The sample was excited with 300 μW of power (before the objective) by a 532 nm continuous-wave diode pumped solid-state laser (Coherent). The laser was focused

227 onto the sample by an oil immersion objective lens (Olympus 100x; numerical
228 aperture 1.3). The light emitted from the sample was recollected using the same
229 objective and the green light from the excitation laser was filtered out of the detection
230 channel using a 550 nm long pass filter (Thorlabs). The light was collected by a
231 commercial spectrum analyzer (Princeton Instruments Acton 2500i, Camera Pixis
232 100). Spectra were collected for 30 seconds using a grating with 300 groves/mm
233 blazed at 750 nm. Alternatively, a 685 nm continuous-wave diode laser (Newport), in
234 the same setup but with the addition of a 700 nm long pass filter (Thorlabs) was used.
235
236 Carbon-isotope data were collected on a Cameca IMS 1280 ion probe
237 (Canadian Center for Isotopic Microanalysis (CCIM), University of Alberta). In total,
238 217 data points were recorded on 7 of the 13 samples; MC02, MC03, MC04, MC06,
239 MC07, MC08 and MC09. The samples were mounted next to a piece of the CCIM
240 synthetic diamond reference material (S0011B and C combustion reference value
241 $\delta^{13}C_{VPDB}$ = -22.58 ‰), in an indium matrix contained within a 25 mm diameter brass
242 mount. The reported propagated uncertainties include within-spot and between-spot
243 statistical measurements and those associated with IMF correction, and are typically
244 ±0.15 ‰ (95% confidence level). The carbon-isotope data are reported as $1000 \times \delta^{13}C$
245 relative to VPDB ($^{13}C/^{12}C$ = 0.001118).
246
247 **RESULTS**
248
249 Note that in this study, the term cuboid is used to refer to the type of diamond
250 growth as defined by Moore & Lang (1972) and does not refer in any way to the
251 morphology or habit of the diamond crystal. While it is conceded that natural

252 diamonds, in general, do not form perfect cube habits, the term cube will be used in
253 this study to refer to roughly cube-like morphologies.
254
255 **General optical, crystallographic and CL characteristics**
256
257 EBSD analysis reveals that eleven of the thirteen diamond plates are cut to
258 within 10^{o} of perpendicular to a [100] axis; samples MC03 and MC05 are cut
259 perpendicular to a [110] axis. The arrows marked on **Fig. 2** show the crystallographic
260 orientations of the [100] axes for all the samples. In general, the optically dark regions
261 are in the [100] direction (i.e. octahedral sectors), and the transparent diamond is in
262 the [111] direction (i.e. cuboid sectors). Within an individual diamond sample,
263 variations in the orientation of the crystal lattice are below the detection limit of the
264 EBSD technique. No lattice misorientations could be detected between the octahedral
265 and cuboid sectors. For a few of the samples with a more complex growth history
266 (MC04, 05, 06, 12), the light-scattering defects in the dark regions define concentric
267 patterns, which results from cuboid growth becoming dominant over the octahedral
268 growth (see **Fig.1 and 2**).
269 All the diamonds emit green CL from the cuboid sectors when examined using
270 the luminoscope system. However, this system is not sensitive enough to observe any
271 emissions from the octahedral sectors. The black and white CL images obtained from
272 the SEM have much greater contrast so more detail can be obtained from the more
273 weakly-luminescent octahedral sectors (**Fig. 4a – b,** MC03). Some of the samples
274 (MC01, 10 and 13; **Fig. 4c – d**) show no growth stratigraphy perpendicular to the
275 growth direction, and the CL only reveals boundaries between the octahedral and
276 cuboid sectors (parallel to the growth direction). All the other samples show varying

277 amounts of stratigraphy, with the growth bands forming perfectly straight lines in the
278 octahedral sectors, and curved hummocky forms in the cuboid sectors (**Fig. 4e** MC02,
279 **4f** MC03, **4g** MC04, **4h** MC08, **4i** MC09, **4j** MC07, **4k** MC06, **4l** MC05). Note also
280 the almost fully spherical forms in the cuboid sectors and the resorption event that
281 occurred towards the outer edge of MC02 (**Fig. 4e**), the triangular forms that develop
282 in the cuboid sectors of MC03 as it transitions to octahedral growth (**Fig. 4a, b, f**), and
283 the small cuboid forms contained within octahedral sectors in MC01, 07 and 09 (**Fig.**
284 **4c, i, j**). Curved features, similar to those seen in MC02, have been described by Seal
285 (1965) as being "*oblique sections through bent but roughly cylindrical domes sloping*
286 *upwards and outwards from a central dimple.*" Ultimately, many of the variations in
287 the center-cross patterns seen in **Fig. 2** relate to the sectioning of the diamond with
288 respect to the growth nucleus. For a full discussion of this subject see Lang (1979).
289
290 **Inferred Growth Morphology**
291
292 As the diamonds were obtained as doubly polished plates, information about
293 their original morphology has to be inferred from their current form. The following
294 inferred growth histories are based on the CL pattern of the stones and the assumption
295 that the outer edges of the plates are still representative of the stones' original
296 morphology. Of the seven plates with approximately square outlines, four are inferred
297 to have had an octahedral morphology (MC02, 05, 07 and 10) because the <100>
298 crystallographic directions and light-scattering defects are directed to the corners (**Fig.**
299 **1c**). The growth of MC02 (**Fig.2 and 4e**) is fairly uniform, with the cuboid sectors
300 maintaining a consistent width except towards the outer edge, where there is an
301 indication of a resorption event. Of the other three specimens, MC05's growth

appears to be quite complex (**Fig. 4l**), but this may be a result of the specimen not being cut parallel to a growth direction. MC07 is dominated by cuboid growth in the early stages but less so later in its growth (**Fig. 4j**), and MC10 is very similar to that of MC02, with fairly constant ratios of octahedral to cuboid growth (**Fig. 2**). MC03, also of octahedral morphology but with a more lozenge-shaped appearance, (**Fig.2 and 4a, b, f**) shows a very complex growth history. At the core of the stone it was cuboid-dominated, and then the stone became more equally mixed-habit. Towards the end, octahedral growth totally dominated and this is best revealed by the pyramid features in the CL pattern (**Fig. 4b**). These represent octahedral facets starting to form within the cuboid sectors.

The remaining three diamonds with roughly square outlines (MC04, 06 and 11) are inferred to have had a cubic morphology as the <111> crystallographic directions are towards the corners (**Fig. 1b and 2**). MC04 has octahedral facets almost totally grown out, while CL imaging of MC06 (**Fig. 4k**) shows that cuboid growth totally dominates the outer part of the stone despite it being partially resorbed. This stone also shows how the CL patterns of the sectors vary dramatically when cut well off a <100> direction (Lang, 1979). In sample MC11 (**Fig. 2**) cuboid growth dominates, but two octahedral sectors reach the edge of the stone without diminishing in volume. One rounded sample, MC09 (**Fig 2 and 4i**) is also dominated by cuboid growth.

Of the remaining four samples (MC01, 08, 12 and 13), two have rounded morphology (**Fig. 4h**) and two are octahedral with re-entrants in the <100> directions (**Fig. 2**), but they all contain fairly equal volumes of mixed-habit growth.

IR Spectroscopy

Averaged nitrogen, hydrogen and platelet data for each sector of the thirteen diamonds are shown in **Table 1**. It is clear that nitrogen concentrations are very high (>1400 ppm) in all thirteen diamonds, and that the octahedral sectors are more enriched than the cuboid ones. Overall, nitrogen aggregation is relatively low for all sectors (3 – 23 % IaB, median 12% IaB). The nitrogen-aggregation data appear to suggest that in all but one case, cuboid sectors are more aggregated than the octahedral ones. The hydrogen concentrations are only high in the cuboid sectors; the main band at 3107 cm^{-1} and the secondary band at 1405 cm^{-1} are accompanied by bands at 3051, 3143, 3188, 3236 and 3309 cm^{-1}. Hydrogen measurements were compiled into IR maps as it is unaffected by the nitrogen-related saturation and the maps of four samples are shown in **Fig. 5**.

Of the five diamonds with octahedral morphology, MC07 and MC10 contain no platelets in any sector, MC03 and MC05 have low platelet intensities (8 – 13 cm^{-2}) in only the cuboid sectors, and MC02 has a high platelet intensity (~200 cm^{-2}) but only in the octahedral sectors (see **Table 1**). Samples MC03 and MC05 also show interesting variations in the nitrogen concentration because their growth mechanisms vary. In both cases, as the cuboid sectors transition to octahedral growth, nitrogen concentrations drop from ~1950 ppm to as low as 1200 ppm in MC03 (**Fig. 6**), while in MC05 they drop from ~2050 ppm in the core to ~1480 ppm towards the rim.

In the four diamonds whose growth is cuboid-dominated, small platelet intensities (~5 – 10 cm^{-2}) are recorded only in the cuboid sectors of MC06 and MC09, and MC11 contains no platelets in any sector. MC04 has small platelet intensities in both cuboid (7 cm^{-2}) and octahedral (2 cm^{-2}) sectors. There is also a decrease in the

nitrogen concentrations of both sectors as cuboid growth becomes dominant (see MC04 in **Fig. 6**).

The final four diamonds all exhibit fairly equal proportions of mixed-habit growth; MC13 contains no platelets in any sector, while MC01, MC08 and MC12 have small platelet intensities (~5 – 14 cm^{-2}) only in the cuboid sectors.

In summary, all of the diamonds except two either have platelets in only the cuboid sectors, or have no platelets in any sector. MC04 contains a small platelet feature in both sectors, while MC02 is the only sample to have a large platelet band and that only occurs in the octahedral sectors. When one growth mechanism becomes dominant over the other, the change is accompanied by a drop in nitrogen concentrations in both octahedral and cuboid sectors, regardless of which type of growth is becoming dominant.

The final feature of interest is the small broad band around 1580 cm^{-1}. This feature, seen only in cuboid sectors, was observed in eight of the samples and is, according to Nemanich et al. (1977), related to graphite. The absence of other spectral features confirms that the *disc-crack-like* defects of the cuboid sectors do not contain fluid or silicate mineral inclusions.

Raman and Photoluminescence Spectroscopy

Raman and PL analyses, especially those placed in the cuboid sectors, were complicated by strong laser-induced, broad-band luminescence of unknown origin. Raman analyses of the *disc-crack-like* defects in the cuboid sectors revealed that they are in fact graphite, as previously shown by Rondeau et al. (2004) and suggested by Lang et al. (2007). The graphite G band near 1580 cm^{-1} (for the band assignment see

Tuinstra and Koenig, 1970) was found to be relatively narrow (full width half maximum [FWHM] values in the range 13.4–25.4 cm^{-1}). This observation suggests that the graphite is well crystallized to, at the most, moderately disordered (compare Beyssac et al., 2002; Nasdala et al., 2003). Raman analyses of the diamond regions immediately surrounding these graphite bodies yielded spectra with a mildly broadened, always somewhat asymmetric main first-order diamond band at 1332.0–1333.8 cm^{-1}. The slight up-shift with respect to the diamond host (~1332.0 cm^{-1}) indicates that the graphite transmits a small amount of compressive stress (Sharma et al., 1985; Nasdala et al., 2005) to the diamond host. This is consistent with the TEM study of these types of defects by Walmsley et al. (1987).

Two excitation wavelengths were used in the PL work in order to avoid, at least partially, the broad luminescence background. A band at ~794 nm was observed only in the cuboid sectors of the diamonds (**Fig.7**). This feature may be assigned to the Zero Phonon Line (ZPL) of the S2 and S3 nickel centers (Kupriyanov et al., 1999), also known as the NE2 and NE1 electron paramagnetic resonance centers (Lang et al., 2004). Spectra obtained in the cuboid sectors with 532 nm excitation showed two additional bands at ~706 and ~658 nm. These are most probably also related to nickel impurities as their positions are very close to the nickel-induced CL emission at 703.6 nm (Nadolinny et al., 1999) and PL emission at 658.3 nm (Yelisseyev et al., 1996) respectively.

Carbon Isotopes

Of the 217 analyses performed on seven samples, the total range of $\delta^{13}C$ is -7.94 to -9.61 ‰ (**Supplementary Data**). The largest range seen in a single sample,

MC03, is 0.98 ‰ (-8.63 to -9.61 ‰). The most thoroughly studied sample, MC07, with 69 analyses transecting both octahedral and cuboid sectors (**Fig. 4j**), shows a slight trend to less negative $\delta^{13}C$ values moving from the core to the rim. This change occurs in both sectors, with no significant difference in the $\delta^{13}C$ values between the two. A similar slight increase in $\delta^{13}C$ values is also seen in the cuboid sector of MC03 (**Fig. 8a**). In the remaining samples, MC02, 04, 06, 08 and 09, no $\delta^{13}C$ variation between core and rim was noted. To confirm that no fractionation occurs between sectors, nine pairs of analyses of contemporary growth horizons were performed on MC06 (**Fig. 4k**), with spots in each sector of the same growth layer. None of the analyses show any statistical difference between sectors (**Fig. 8b**) and therefore there is no evidence of carbon-isotope fractionation between the sectors.

DISCUSSION

Impurity Characteristics

The most commonly reported characteristic of mixed-habit diamonds relates to their high nitrogen concentrations (e.g. Welbourn et al., 1989; Bulanova et al., 2002; Rondeau et al., 2004). That result is supported in this study, with overall nitrogen concentrations ranging from 1400 – 2700 ppm, and nitrogen enriched in the octahedral sectors compared to contemporary cuboid sectors by 127 – 143 % (**Table 1**). Differences between the moderately low levels of nitrogen aggregation in both sectors are more difficult to assess due to the saturation of the spectra in the nitrogen-dominated region (1000 – 1350 cm^{-1}). In most cases, the data initially suggest that aggregation levels are higher in the cuboid sectors. Considering their lower

426 concentrations, this implies a faster rate of nitrogen aggregation in cuboid diamond
427 than octahedral diamond. However, the deconvolution method applied to saturated
428 spectra significantly under-represents the B center component (see Analytical
429 Techniques section) and this has a greater affect on the data from the octahedral
430 sectors. Taking this uncertainty in to account, we believe that there is no significant
431 difference in nitrogen aggregation levels between the two sectors. It is not possible to
432 determine whether this means that aggregation does occur at significantly faster rates
433 in cuboid diamond growth, but it is assumed it does not.

434 If nitrogen aggregation occurs at the same rate in both octahedral and cuboid
435 diamond growth, then interstitial carbon atoms are also being generated at the same
436 rate (Woods, 1986). These interstitial carbon atoms aggregate together very quickly to
437 form platelets. This relationship between B centers and interstitial carbon atoms
438 results in a linear trend between the integrated area of the platelet (B′) peak and the
439 amount of IR absorption caused by B centers (Woods, 1986). When the
440 proportionality between the integrated intensity and the IR absorption is less than the
441 expected coefficient from the general linear trend, it usually is interpreted as being
442 due to the degradation of the platelets caused by heating and/or deformation events
443 (Woods, 1986).

444 This linear relationship established by Woods (1986) means that the constant
445 rate of nitrogen aggregation, combined with nitrogen enrichment in the octahedral
446 sectors should result in proportionally larger platelet intensities in the octahedral
447 sectors of mixed-habit diamonds. In other words, more nitrogen creates more B
448 centers, which in turn create more interstitial carbon atoms and therefore more / larger
449 platelets. However, the I(B′) data from mixed-habit diamonds in both the literature
450 (e.g. Welbourn et al., 1989; Bulanova et al., 2002; Rondeau et al., 2004; Howell et al.,

2012b) and this study, show no consistency with regard to sector variations. For example, platelets may occur in just one sector, or have higher intensities in one sector compared to the other.

To explain this phenomenon, we consider both how platelets form, and how they degrade. There have been two proposals regarding nitrogen aggregation and platelet formation in mixed-habit diamonds. Rondeau et al. (2004) suggested that nitrogen aggregation is impeded in cuboid sectors due to hydrogen being bonded to the A center defects. Reduced aggregation to B centers means fewer interstitial carbon atoms are generated and fewer platelets created. Conversely, Howell et al. (2012b) proposed that nitrogen aggregation rates were the same in both sectors, but the interstitial carbon atoms interacted with the *disc-crack-like* defects in the cuboid sectors (Walmsley et al., 1987). This would reduce their likelihood of aggregating to form platelets, but would not totally prevent it, as not all the interstitial carbon atoms would interact with the defects. This means that the linear relationship of Woods (1986) would not be applicable to cuboid diamond growth, as the concentration of the *disc-crack-like* defects needs to be taken into account. As we see no difference in the nitrogen aggregation rates between the sectors (if anything nitrogen aggregation may occur faster in cuboid diamond), data from the present work support the conclusions of Howell et al. (2012b).

To explain the diversity of platelet features seen in mixed-habit diamonds, we also need to understand how platelets are degraded. The main mechanism for platelet degradation is dislocation-related (Hirsch et al., 1986) and it has a stronger effect on larger platelets than on smaller ones (Lang et al., 2007). The IR data available for platelets in mixed-habit diamonds (Lang et al., 2007; Howell et al., 2012b) show that platelets in octahedral sectors have a greater area per unit volume (Sumida & Lang,

476 1988) and larger mean radius (Clackson et al., 1990) compared to those in cuboid
477 sectors. Therefore, not only do platelets form more rapidly in octahedral sectors, they
478 will also degrade more easily.

479 Deformation and/or heating events are intrinsic to the degradation of platelets
480 (Woods, 1986). This is because the mechanism requires either the generation of
481 dislocations, or mobilization of existing ones, to create the loops that produce the
482 vacancies necessary for platelet decomposition (Hirsch et al., 1986). None of the
483 thirteen diamonds in this study shows any visual evidence of being plastically
484 deformed; this is supported by their crystallographic homogeneity as recorded by the
485 EBSD analysis. However, the graphitization of the *disc-crack-like* defects (see earlier)
486 is evidence that the diamonds have experienced a heating event at some point in their
487 history (Howes, 1962; Evans, 1979). This heating would allow the platelet data from
488 the diamonds in this study to be explained simply by varying the timing and intensity
489 of the heating event. For example, a brief heating event just prior to volcanic
490 exhumation would reduce the larger platelet features of the octahedral sector, while
491 the smaller platelet features in the cuboid sector would be less affected. This would
492 result in small platelet features in both sectors. Increasing the duration and/or
493 temperature of the heating event would initially cause further degradation of the
494 octahedral platelets, so that platelets only survived in the cuboid sectors. If the heating
495 event persisted, total degradation of the platelets in the cuboid sectors would also
496 occur, leaving no platelets in either sector despite aggregation levels of up to 15 %
497 IaB. Alternatively, a significant heating event that occurred well before exhumation
498 would initially result in total platelet degradation in both sectors, but there would be
499 time for subsequent platelet development to occur. Depending on the concentration of
500 the *disc-crack-like* defects in the cuboid sectors, this could result in only a large

501 platelet feature being observed in the octahedral sector, as platelet development in the
502 cuboid sector remains impeded by the defects.

503 Another common characteristic of mixed-habit diamonds noted in the
504 literature is the presence of significant levels of IR-active hydrogen, principally in the
505 cuboid sectors only. The diamonds in this study show strong IR-active hydrogen
506 features in the cuboid sectors (25 – 77 cm^{-1}; **Table 1**), although commonly there is a
507 much weaker feature in the octahedral sectors (< 11 cm^{-1}) as well. Other than the
508 *disc-crack-like* defects, there are no defects that only occur in the cuboid sectors to
509 offer suitable sites for IR-active hydrogen bonding. Therefore the data from this study
510 suggest that hydrogen is bound to the diamond at the surfaces of these defects in the
511 cuboid sectors, as proposed by Howell et al. (2012b) and in accordance with the
512 suggestion of Woods & Collins (1983). It is possible that a small contribution to the
513 3107 cm^{-1} band comes from hydrogen residing at nitrogen-related defects (Rondeau
514 et al., 2004). As this would occur in both sectors, it would explain the smaller
515 hydrogen-related bands seen in the octahedral sectors.

516 As the intensity of the hydrogen-related IR feature does not correlate with the
517 actual hydrogen concentration within the diamond as a whole (Sweeney et al., 1999),
518 the exact role of hydrogen in diamond is not fully understood. An investigation of
519 whether differences in total hydrogen concentrations exist or not, and whether
520 hydrogen partitions between both sectors or is concentrated mainly in one type of
521 sector could provide new insights into mixed-habit diamond formation.

522 The final impurity to discuss is nickel, which is present in the cuboid sectors.
523 This element is responsible for the green cathodoluminescence that is commonly
524 observed in mixed-habit diamonds (Welbourn et al., 1989), including all of those
525 studied here. No nickel concentrations have yet been measured in mixed-habit

526 diamonds, but Lang et al. (2004) suggest that concentrations would be < 0.1 ppm.
527 More recent laser-ablation studies have reported nickel concentrations up to 0.3 ppm
528 in monocrystalline diamonds (Rege et al., 2010).

529 It has been observed that nickel enhances nitrogen aggregation in synthetic
530 diamonds (Kiflawi et al., 1998; Fisher and Lawson, 1998) and these authors propose
531 two reasons: (1) the release of vacancies from the nickel-vacancy complexes, which
532 subsequently assist nitrogen migration; (2) the release of carbon interstitials that in
533 turn release highly mobile nitrogen interstitials. While these mechanisms have only
534 been shown to be of importance for aggregation from C centers to A centers, it is
535 important to recognize that they may also effect aggregation from A to B centers as
536 well, therefore undermining the general relationship to mantle residence time and/or
537 temperature that nitrogen aggregation data are thought to provide.

538

539 **Growth Conditions of Mixed-Habit Diamonds**

540

541 The large body of carbon-isotope data collected in this study shows that the
542 seven samples are very limited in their range, only -7.94 to -9.61 ‰; the largest range
543 in a single sample is only 0.98 ‰ (**Fig. 8a**), and none of the diamonds shows strong
544 trends in $\delta^{13}C$ from core to rim. Even the detailed analysis of MC06, designed to
545 identify any fractionation between growth sectors, showed that none existed (**Fig. 8b**).
546 Previous carbon-isotope data from mixed-habit diamonds have almost all been close
547 to the mantle range ($\delta^{13}C$ = -5 to -8 ‰) with three diamonds falling in the range -3 to
548 -7 ‰ (Bulanova et al., 2002; Zedgenizov & Harte, 2004; Howell et al., 2012b). One
549 diamond from SE Australia had a $\delta^{13}C$ = +1.94 ‰, consistent with data for other
550 diamonds from the same location (Cartigny et al., 2003).

As there are no paragenesis-defining inclusions within any of the samples studied, it is not possible to deduce with certainty whether they formed in eclogitic or peridotitic hosts. Considering our data in terms of carbon-isotope and nitrogen-concentration co-variations however, the present data fall very close to a calculated melt evolution trend based on eclogitic diamond growth during reduction of carbonates, with previous loss of a ^{13}C- enriched, nitrogen-bearing CO_2 fluid (Cartigny et al., 2001; Maruoka et al. 2004). The high nitrogen contents of our samples, combined with $\delta^{13}C$ distinctly below the mantle value of ~-5‰ (see Deines, 2002), means that these data fall far off predicted Rayleigh fractionation trends for the precipitation of peridotitic diamonds from reducing (CH_4-bearing) or oxidizing (CO_3^{2-}-bearing) fluids (see Figure 7 of Stachel & Harris, 2009). However, there is a subset of peridotitic coated diamonds with initial $\delta^{13}C$ values as low as -9‰, consistent with carbonate precipitation (Stachel et al., 2009). So while the evidence points to an eclogitic paragenesis there is the lesser possibility of an origin from a ^{13}C-depleted carbonate-bearing fluid in a peridotitic environment (Stachel et al., 2009). The presence of nickel in the diamonds implies the absence of sulphides during diamond formation (as sulfides would scavenge all the nickel) and this evidence could favor diamond formation in a Ni-rich depleted cratonic peridotite.

Two of the diamonds exhibit a significant change in nitrogen concentration from the core to the rim (MC03 & MC04, **Fig. 6**). This variation correlates with a change in growth type, with octahedral growth becoming dominant in MC03 and cuboid growth dominating in MC04. Neither of these samples shows an accompanying trend in carbon isotopes, ruling out growth from a closed system. Redox reactions and/or the absorption of impurities are the key factors in allowing mixed-habit growth to occur and be sustained (see Introduction). If growth occurs in

an open system, then in general, for large volumes of mixed-habit growth to occur the physiochemical conditions must be very stable, as only a slight change will result in one growth type becoming dominant. In the present case, such an argument is supported by the lack of variation in carbon isotopes and the sustained impurity concentrations in the majority of the diamonds studied. With MC03 and MC04, a change in the impurity concentration of the source fluid seems most likely, resulting in growth moving away from mixed-habit and becoming dominated by just one type. If the model of Howell et al. (2012b) is correct, then a drop in hydrogen concentrations may have caused octahedral growth to become dominant in MC03 (the accompanying drop in nitrogen being irrelevant), while a drop in nitrogen concentration with continued high hydrogen concentrations may have caused cuboid growth to dominate in MC04 (**Fig. 9**).

To summarize, the data collected from this set of mixed-habit diamonds suggests that growth occurred under the following conditions; (1) relatively constant pressure (P) and temperature (T), (2) sustained levels of carbon super-saturation, (3) a relatively high nitrogen concentration in the source fluid, and (4) a reduced oxygen fugacity (fO_2) providing diamond-forming carbon through the reduction of carbonates. The role and importance of hydrogen to mixed-habit and particularly cuboid growth remain uncertain but would be clarified if actual concentrations and sectoral variations were confirmed. The role that nickel plays in cuboid diamond growth is also uncertain, but it is not deemed integral to mixed-habit growth.

The data from this study support the following preliminary model for mixed-habit diamond crystal growth. High concentrations of nitrogen and hydrogen in the source fluid are the key factors required for mixed-habit growth to occur (Rondeau et al., 2004; Howell et al., 2012b). Nitrogen is preferentially taken up in the octahedral

sectors, while hydrogen is better accommodated in the cuboid sectors. Other important factors like P, T, fO_2, and carbon saturation must remain fairly constant to avoid driving the growth conditions away from mixed-habit growth.

Mixed-habit diamonds may be under-represented in population studies because the cross feature is only visible if the *disc-crack-like* defects have been graphitized. Their rarity may also be linked to the very stable conditions required for their growth. If that is the case, then appropriate growth conditions may only be encountered for brief periods. The consequence of this would be that only small volumes of mixed-habit growth will occur during transitions (in either direction) from octahedral to cuboid growth (e.g. Kaminsky & Khachatryan, 2004; Skuzovatov et al., 2011; Howell et al., 2012a, b)

CONCLUSIONS

This study has presented a large body of spectroscopic and carbon-isotope data on mixed-habit diamonds, significantly increasing the current dataset. These data help to reinforce new ideas regarding the behaviour of various impurities in diamond, namely the rates of nitrogen aggregation and subsequent platelet development in octahedral and cuboid sectors, and the presence of significant IR-active hydrogen principally in cuboid sectors. The highly crystalline state of the graphite coating the *disc-crack-like* defects, and the residual strain surrounding them, support the interpretation that graphitization occurred during heating events subsequent to diamond formation in the mantle. The presence of nickel in the cuboid sectors, creating green CL, probably indicates the absence of any sulphide phase during diamond growth. An origin for mixed-habit diamonds during carbonate reduction is

626 proposed, supporting an earlier hypothesis (Howell et al., 2012b) that the reducing
627 oxygen-fugacity conditions could also produce the high levels of hydrogen required to
628 sustain cuboid growth. However, both quantitative analysis of hydrogen
629 concentrations in mixed-habit diamonds and HPHT experiments are required to
630 confirm this.
631
632 **ACKNOWLEDGEMENTS**
633
634 John Chapman is thanked for suggesting the data processing method for N-saturated
635 IR spectra and for directing us to the collection of diamonds used in this study. Darren
636 Arthur is thanked for giving us access to these and other mixed-habit samples. O.
637 Beyssac is thanked for discussion regarding the graphite Raman spectra. Jeff Harris
638 and another anonymous reviewer are thanked for their comments that helped improve
639 the manuscript. Boriana Mihailova is thanked for her editorial handling of the
640 manuscript. JMS is supported by a Macquarie Research Excellence International
641 Scholarship and would also like to acknowledge support from the Australian Research
642 Council Discovery Projects scheme (DP1094439) and Centers of Excellence
643 (CE110001013). The authors acknowledge the EBSD facility and technical assistance
644 of the Australian Microscopy & Microanalysis Research Facility at the Australian
645 Centre for Microscopy & Microanalysis, University of Sydney. SIMS analyses were
646 conducted under Project P1005 of the Canadian Center for Isotopic Microanalysis.
647 Some of the analytical work used instrumentation in the Geochemical Analysis Unit
648 (GAU) of the GEMOC Key Center, funded by DEST Systemic Infrastructure Grants,
649 ARC LIEF, NCRIS, industry partners and Macquarie University. This is contribution
650 178 from the ARC Center of Excellence for Core to Crust Fluid Systems

(www.ccfs.mq.edu.au) and 826 from the GEMOC Key Center (www.gemoc.mq.edu.au). The DiaMap routine used in this study can be downloaded, along with instructions, from the GEMOC website.

REFERENCES CITED

Araujo, D.P., Griffin, W.L., O'Reilly, S.Y., Grant, K.J., Ireland, T., Holden, P., and van Achterbergh, E. (2009) Microinclusions in monocrystalline octahedral diamonds and coated diamonds from Diavik, Slave Craton: Clues to diamond genesis. Lithos, 112S, 724–735.

Beyssac, O., Goffé, B., Petitet, J.P., Froigneux, E., Moreau, M., and Rouzaud, J.N. (2003) On the characterization of disordered and heterogeneous carbonaceous materials using Raman spectroscopy. Spectrochimica Acta A, 59, 2267–2276.

Boyd, S.R., Pillinger, C.T., Milledge, H.J., Mendelssohn, M.J., and Seal, M. (1988) Fractionation of nitrogen isotopes in a synthetic diamond of mixed crystal habit. Nature, 331, 604–607.

Boyd, S.R., Pillinger, C.T., Milledge, H.J., Mendelssohn, M.J., and Seal, M. (1992) C and N isotopic composition and the infrared absorption spectra of coated diamonds: evidence for the regional uniformity of CO_2-H_2O rich fluids in lithospheric mantle. Earth and Planetary Science Letters, 109, 633–644.

Boyd, S.R., Kiflawi, I., and Woods, G.S. (1994) The relationship between infrared absorption and the A defect concentration in diamond. Philosophical Magazine B, 69, 1149-1153.

Boyd, S.R., Kiflawi, I., and Woods, G.S. (1995) Infrared absorption by the B nitrogen aggregate in diamond. Philosophical Magazine B, 72, 351-361.

Bradac, C., Gaebel, T., Naidoo, N., Rabeau J.R., and Barnard, A.S. (2009) Prediction and Measurement of the Size-Dependent Stability of Fluorescence in Diamond over the Entire Nanoscale. Nano Letters, 9, 3555–3564.

Bulanova, G.P., Pearson, D.G., Hauri, E.H., and Griffin, B.J. (2002) Carbon and nitrogen isotope systematics with a sector-growth diamond from the Mir kimberlite, Yakutia. Chemical Geology, 188, 105–123.

Cartigny, P., Harris, J.W., and Javoy, M. (2001) Diamond genesis, mantle fractionations and mantle nitrogen content: a study of δ^{13}C-N concentrations in diamonds. Earth and Planetary Science Letters, 185, 85–98.

Cartigny, P., Harris, J.W., Taylor, A., Davies, R., and Javoy, M. (2003) On the possibility of a kinetic fractionation of nitrogen stable isotopes during natural diamond growth. Geochimica et Cosmochimica Acta, 67, 1571–1576.

Clackson S.G., Moore M., Walmsley J.C., and Woods G.S. (1990) The relationship between platelet size and frequency of the B' infrared absorption peak in Type Ia diamond. Philosophical Magazine B, 62, 115-128.

Deines, P. (2002) The carbon isotope geochemistry of mantle xenoliths. Earth-Science Reviews, 58, 247-278.

Evans, T. (1979) Changes produced by high temperature treatment of diamond. In: Fields J (ed) The properties of diamond. Academic Press, London, pp 403–424.

Fisher, D., and Lawson, S.C. (1998) The effect of nickel and cobalt on the aggregation of nitrogen in diamond. Diamond and Related Materials, 7, 299-304.

Frank, F.C. (1967) Defects in diamond. In: Burls J (ed) Science and Technology of Industrial Diamonds, vol. 1. Industrial Diamond Information Bureau, London, pp 119–135

Harrison, E.R. and Tolansky, S. (1964) Growth history of a natural octahedral diamond. Proceedings of the Royal Society of London A, 279, 490–496.

Hirsch, P.B., Pirouz, P., and Barry, J.C. (1986) Platelets, dislocation loops and voidites in diamond. Proceedings of the Royal Society of London A, 407, 239–258

Howell, D., O'Neill, C.J., Grant, K.J., Griffin, W.L., Pearson, N.J., and O'Reilly S.Y. (2012 a). μ-FTIR mapping: Distribution of impurities in different types of diamond growth. Accepted, Diamond and Related Materials.

Howell, D., O'Neill, C.J., Grant, K.J., Griffin, W.L., Pearson, N.J., O'Reilly S.Y., Stern R., and Stachel T. (2012 b). Platelet development in cuboid diamonds: insights from μ-FTIR mapping. Accepted Contributions to Mineralogy and Petrology.

Howes, V.R. (1962) The graphitization of diamond. Proceedings of the Physics Society, 80, 648-662.

715 Kaminsky, F.V., and Khachatryan, G.K. (2004) The relationship between the
716 distribution of nitrogen impurity centres in diamond crystals and their internal
717 structure and mechanism of growth. Lithos, 77, 255–271
718 Kiflawi, I., Kanda H., and Mainwood, A. (1998) The effect of nickel and the kinetics
719 of the aggregation of nitrogen in diamond. Diamond and Related Materials, 7,
720 327–332.
721 Kupriyanov, I.N., Gusev, V.A., Borzdov, Y.M., Kalinin, A.A., and Palyanov, Y.N.
722 (1999) Photoluminescence study of annealed nickel- and nitrogen-containing
723 synthetic diamond. Diamond and Related Materials, 8, 1301–1309.
724 Lang, A.R. (1974) On the growth-sectorial dependence of defects in natural
725 diamonds. Proceedings of the Royal Society of London A, 340, 233–248
726 Lang, A.R. (1979) Internal structure. In: Fields J (ed) The properties of diamond.
727 Academic Press, London, pp 425–469
728 Lang, A.R., Bulanova, G.P., Fisher, D., Furkert, S., and Sarua, A. (2007) Defects in a
729 mixed-habit Yakutian diamond: studies by optical and cathodoluminescence
730 microscopy, infrared absorption, Raman scattering and photoluminescence
731 spectroscopy. Journal of Crystal Growth, 309, 170–180.
732 Lang, A.R., Yelisseyev, A.P., Pokhilenko, N.P., Steeds, J.W., and Wotherspoon, A.
733 (2004) Is dispersed nickel in natural diamonds associated with cuboid growth
734 sectors in diamonds that exhibit a history of mixed-habit growth? Journal of
735 Crystal Growth, 263, 575–589.
736 Maruoka, T., Kurat, G., Dobosi, G., and Koeberl, C. (2004). Isotopic composition of
737 carbon in diamonds from diamondites: record of mass fractionation in the upper
738 mantle. Geochimica et Cosmochimica Acta, 68, 1635–1644.
739 Moore, M., and Lang, A.R. (1972) Internal structure of natural diamonds of cubic
740 habit. Philosophical Magazine, 26(6), 1313–1325.
741 Nadolinny, V.A., Yelisseyev, A.P., Baker, J.M., Newton, M.E., Twitchen, D.J.,
742 Lawson, S.C., Yuryeva, O.P., and Feigelson, B.N. (1999) A study of 13C
743 hyperfine structure in the EPR of nickel-nitrogen-containing centres in diamond
744 and correlation with their optical properties. Journal of Physics: Condensed
745 Matter, 11, 7357–7376.
746 Nasdala, L., Brenker, F.E., Glinnemann, J., Hofmeister, W., Gasparik, T., Harris,
747 J.W., Stachel, T, and Reese, I. (2003) Spectroscopic 2D-tomography: Residual

748 pressure and strain around mineral inclusions in diamonds. European Journal of
749 Mineralogy, 15, 931–935.
750 Nasdala, L., Hofmeister, W., Harris, J.W., and Glinnemann, J. (2005): Growth zoning
751 and strain patterns inside diamond crystals as revealed by Raman maps.
752 American Mineralogist, 90, 745–748.
753 Nemanich, R.J., Lucovsky, G., and Solin, S.A. (1977) Infrared active optical
754 vibrations of graphite. Solid State Communications, 23, 117–120.
755 Rege, S., Griffin, W.L., Pearson, N.J., Araujo, D.P., Zedgenizov, D.A., and O'Reilly,
756 S.Y. (2010) Trace-element patterns of fibrous and monocrystalline diamonds:
757 Insights into mantle fluids. Lithos, 118, 313–337.
758 Reutsky, V.N., Harte, B., EIMF, Borzdov, Y.M., and Palyanov, Y.N. (2008)
759 Monitoring diamond crystal growth, a combined experimental and SIMS study.
760 European Journal of Mineralogy, 20, 365–374.
761 Rondeau, B., Fritsch, E., Guiraud, M., Chalain, J-P., and Notari, F. (2004) Three
762 historical 'asteriated' hydrogen-rich diamonds: growth history and sector-
763 dependence impurity incorporation. Diamond and Related Materials, 13, 1658–
764 1673.
765 Seal, M. (1965) Structure in diamonds as revealed by etching. American Mineralogist,
766 50, 105–123.
767 Sharma, S.K., Mao, H.K., Bell, P.M., and Xu, J.A. (1985) Measurement of stress in
768 diamond anvils with micro-Raman spectroscopy. Journal of Raman
769 Spectroscopy, 16, 350–352.
770 Skuzovatov, S. Yu., Zedgenizov, D.A., Shatsky, V.S., Ragozin, A.L., and Kuper, K.E.
771 (2011) Composition of cloudy microinclusions in octahedral diamonds from the
772 Internatsional'naya kimberlite pipe (Yakutia). Russian Geology and
773 Geophysics, 52, 85–96.
774 Stachel, T. (2001) Diamonds from the asthenosphere and the transition zone,
775 European Journal of Mineralogy, 13, 883-892.
776 Stachel, T., and Harris, J.W. (2008) The origin of cratonic diamonds – constraints
777 from mineral inclusions, Ore Geology Reviews, 34, 5-32.
778 Stachel, T., and Harris, J.W. (2009) Formation of diamond in the Earth's mantle,
779 Journal of Physics: Condensed Matter, 21, 364206.
780 Stachel, T., Harris, J.W., and Muehlenbachs, K. (2009) Sources of carbon in inclusion
781 bearing diamonds. Lithos, 112 (S2), 625-637.

Sumida N., and Lang A.R. (1988) On the measurement of population density and size of platelets in typa 1a diamond and its implications for platelet structure models. Proceedings of the Royal Society London 419, 235-257.

Sunagawa, I. (1990) Growth and morphology of diamond crystals under stable and metastable conditions. Journal of Crystal Growth, 99(1-4), 1156

Sunagawa, I. (2005) Crystals - Growth, Morphology and Perfection. Cambridge University Press, Cambridge.

Suzuki, S., and Lang, A.R. (1976a) Internal structures of natural diamonds revealing mixed-habit growth. In: Diamond Research, vol. International Diamond Information Bureau, London, pp 39–47

Suzuki, S., and Lang, A.R. (1976b) Occurrences of facetted re-entrants on rounded growth surfaces of natural diamonds. Journal of Crystal Growth, 34, 29–37.

Sweeney, R.J., Prozesky, V.M., Viljoen, K.S., and Connell, S. (1999) The sensitive determination of H in diamond by infrared (FTIR) spectroscopy and micro-elastic-recoil (u-ERDA) techniques. Nuclear Instruments and Methods in Physics Research B, 158, 582–587.

Tomlinson, E., Jones, A.P., and Harris, J.W. (2006) Co-existing fluid and silicate inclusions in mantle diamond, Earth and Planetary Science Letters, 250, 581–595.

Tuinstra, F. and Koenig, J.L. (1970) Raman spectrum of graphite. Journal of Chemical Physics, 53, 1126–1130.

Walmsley, J.C., Lang, A.R., Rooney, M-L.T., and Welbourn, C.M. (1987) Newly observed microscopic planar defects on {111} in natural diamond. Philosophical Magazine Letters, 55, 209–213.

Weiss, Y., Kessel, R., Griffin, W.L., Kiflawi, I., Klein-BenDavid, O., Bell, D.R., Harris, J.W., and Navon, O. (2009) A new model for the evolution of diamond-forming fluids: Evidence from microinclusion-bearing diamonds from Kankan, Guinea. Lithos, 112S, 660–674.

Welbourn, C.M., Rooney, M-L.T., and Evans, D.J.F. (1989) A study of diamond of cube and cube-related shape from the Jwaneng mine. Journal of Crystal Growth, 94, 229–252.

Woods, G.S. (1986) Platelets and the infrared absorption of Type Ia diamonds. Proceedings of the Royal Society London A, 407, 219–238.

Woods, G.S., and Collins, A.T. (1983) Infrared absorption spectra of hydrogen complexes in Type I diamonds. Journal of Physics and Chemistry of Solids, 44, 471–475.

Zedgenizov, D.A., and Harte, B. (2004) Microscale variations of $\delta^{13}C$ and N content within a natural diamond with mixed-habit growth. Chemical Geology, 205, 169–175.

Yelisseyev, A., Nadolinny, V., Feigelson, B., Terentyev, S., and Nosukhin, S. (1996) Spatial distribution of impurity defects in synthetic diamonds obtained by the BARS technology. Diamond and Related Materials, 5, 1113–1117.

Figure Captions:

Figure 1. Illustration showing the formation of the center-cross in mixed-habit diamonds (after Sunagawa, 2005). Octahedral growth is in white, while cuboid growth is in grey. The arrows show the crystallographic <100> and <111> directions of the face-centered cubic cell, which correspond to the preferred growth direction of cuboid and octahedral faces, respectively. (a) Constant growth in both the octahedral and cuboid sectors. This results in the final morphology being of mixed-habit. (b) After three growth layers of constant mixed-habit growth, the growth rate of the octahedral sectors (R_o) increases, resulting in them being grown out of the crystal. The final morphology ends up being roughly cube-shaped. (c) The growth rate of the cuboid sectors (R_c) increases after the first three layers of mixed-habit growth, meaning they are grown out of the crystal. The result is an octahedral morphology.

Figure 2. Images of the thirteen mixed-habit diamonds analysed in this study. All are doubly polished plates. All but two are cut within 10^o of a {100} face, MC03

and MC05 are cut parallel to a {110} face. The black arrows point in a <100> direction. The black bars represent 1mm scales.

Figure 3. Illustration showing how deconvolution of IR spectra is performed when there is saturation in the nitrogen-dominated region. The dashed grey line represents the cut-off level; all data above this are omitted from the sum of the squares fit.

Figure 4. CL images of a selection of the diamonds studied. (a) Color image showing the green luminescence of MC03 while (b) shows the equivalent image observed with the SEM, note the greater detail using the SEM. The two images are from the bottom left hand corner as seen in (f). (c) MC01. (d) MC13. (e) MC02. (f) MC03. (g) MC04. (h) MC08. (i) MC09. (j) MC07. (k) MC06. (l) MC05. The yellow dots in (e) – (k) represent the locations of the SIMS analyses. The white lines in (f) and (g) represent the IR transects presented in Fig. 6. The white scale bars correspond to 0.5 mm in (a) and (b) and to 1 mm in (c) – (l).

Figure 5. FTIR impurity maps showing the intensity of the primary hydrogen-related band at 3107 cm^{-1} in four of the samples. Larger hydrogen bands clearly correlate to the cuboid sectors. In MC06, the hydrogen appears to become concentric; this is where cuboid growth becomes more dominant and the amounts of *disc-crack-like* defects vary in the different growth layers. The black bars represent 1mm scales.

867 **Figure 6.** Graphs showing data from the IR maps of MC03 and MC04. The data are
868 from transects that start at the core of the stone and move out to the rim (white
869 lines in Fig. 3).
870
871 **Figure 7.** Photoluminescence spectra obtained from octahedral (thin lines) and cuboid
872 (thick lines) sectors, using a green (532 nm; green lines) and red (685 nm; red
873 lines) laser. The Raman band of diamond is indicated for both the green and red
874 excitation; it is, as expected, present in each sector. The zero phonon lines
875 (ZPL) of several defects are labeled. Specifically, the ZPL at 794 nm, which
876 was observed with both the lasers excitations, has been attributed to the S2 and
877 S3 nickel-related defects (Kupriyanov et al., 1999).
878
879 **Figure 8.** Carbon isotope data from (a) a transect from core to rim of MC03, and (b)
880 two parallel transects in MC06. The black data marks are from the octahedral
881 sector and the grey data marks are from the same growth horizon in the adjacent
882 cuboid sector. The uncertainties on the data are 2σ. In (b) the distance
883 represented on the *x*-axis refers to the distance between each point in the
884 octahedral sector and does not refer to the distance between the analyses of each
885 pair (Fig. 4k).
886
887 **Figure 9.** Schematic illustration showing the role of impurities in mixed-habit growth.
888 The grey dashed lines represent thresholds that need to be crossed to cause a
889 change in growth mechanism (assuming constant pressure, temperature, oxygen
890 fugacity, carbon supersaturation etc.). A high hydrogen concentration is
891 proposed to be necessary for cuboid growth to occur (Rondeau et al., 2004),

with high nitrogen concentrations necessary for mixed-habit growth to occur. The two arrows show how N and H concentrations probably changed during the growth of MC03 and MC04, resulting in one growth mechanism becoming dominant.

Table 1. Averaged impurity data (nitrogen concentration and aggregation state, primary and secondary hydrogen band intensity, integrated area of the platelet band) of the octahedral and cuboid sectors of each of the thirteen diamonds analysed in this study. For samples MC03, MC04 and MC05, additional data are provided to show how these impurities change from the core compared to the rim of the stone. This is only shown for these three samples as only they show significant variations in growth mechanisms between the core and rim.

Supplementary data. Carbon-isotope data from the 217 SIMS analyses performed on seven of the diamond samples. Where possible FTIR analysis has also been performed on the site of the SIMS spots to show additional impurity data.

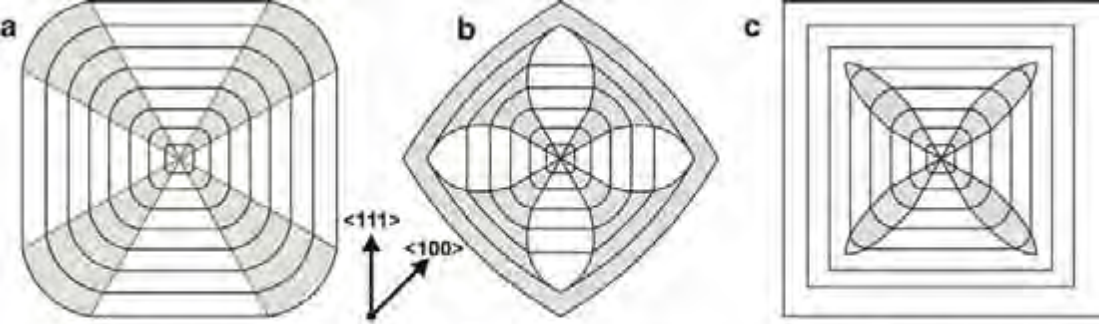
a
b
c
<111>
<100>
R_o & R_c constant
R_o increasing
R_c increasing

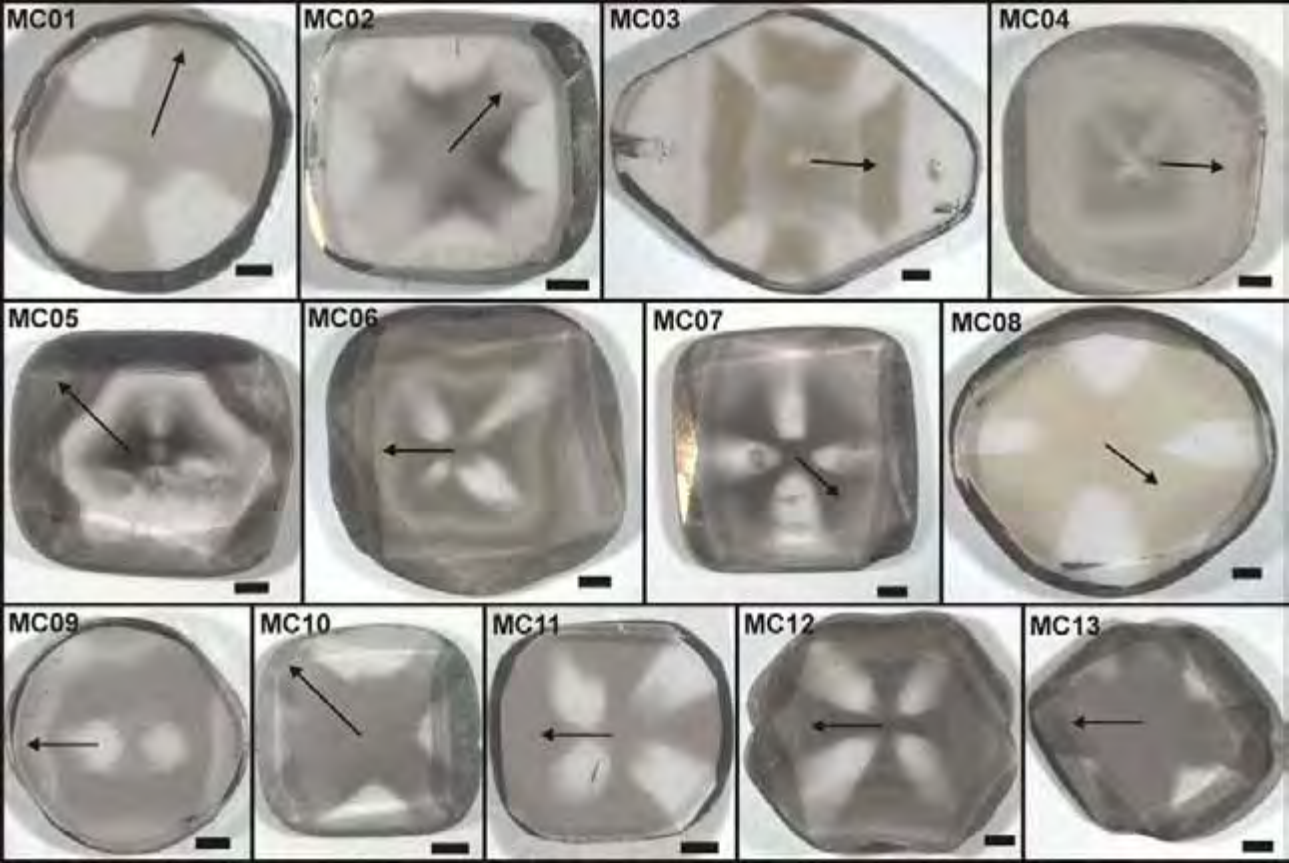
MC01
MC02
MC03
MC04
MC05
MC06
MC07
MC08
MC09
MC10
MC11
MC12
MC13

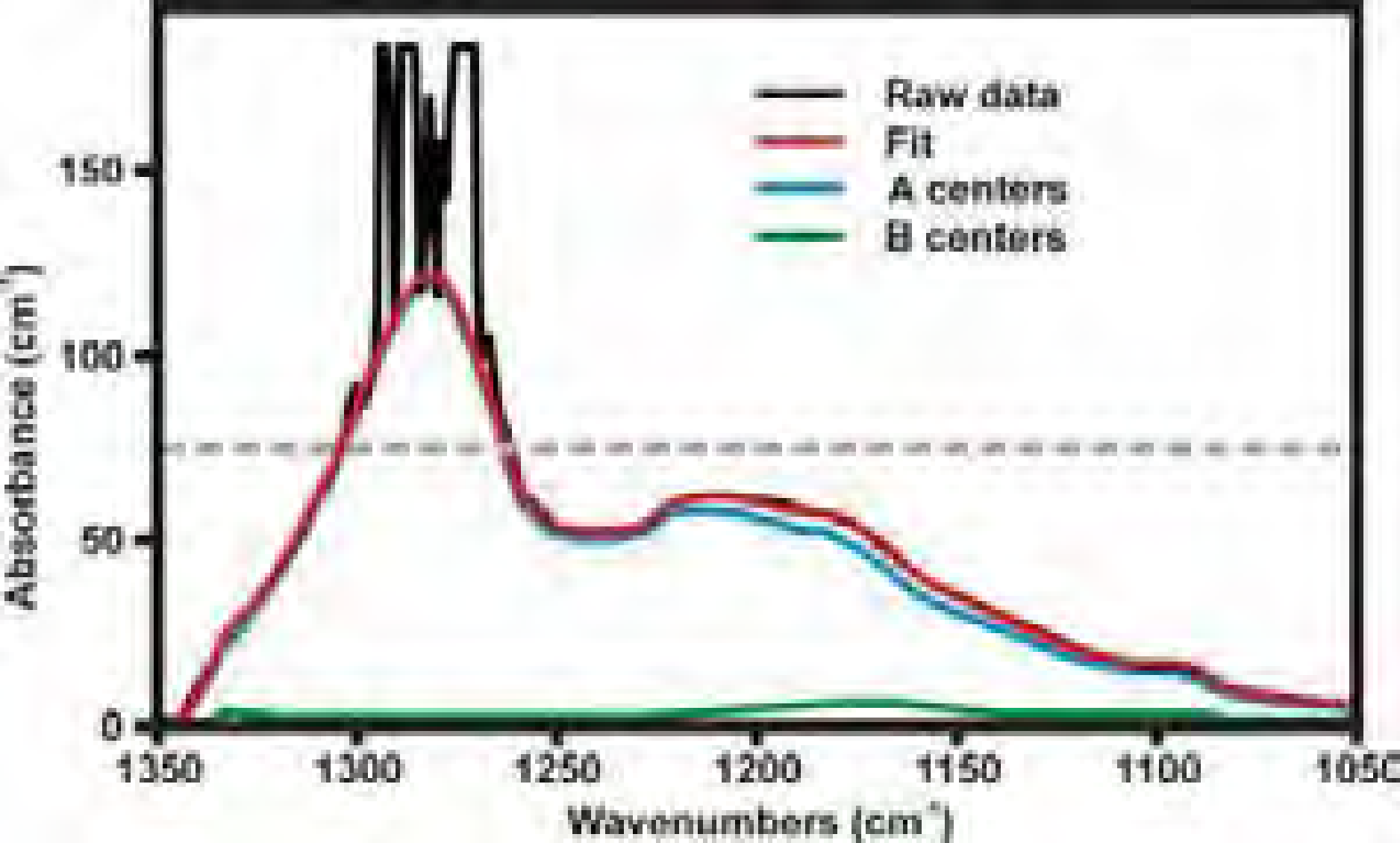
Raw data
Fit
A centers
B centers
150
100
50
0
Absorbance (cm-1)
1350
1300
1250
1200
1150
1100
1050
Wavenumbers (cm-1)

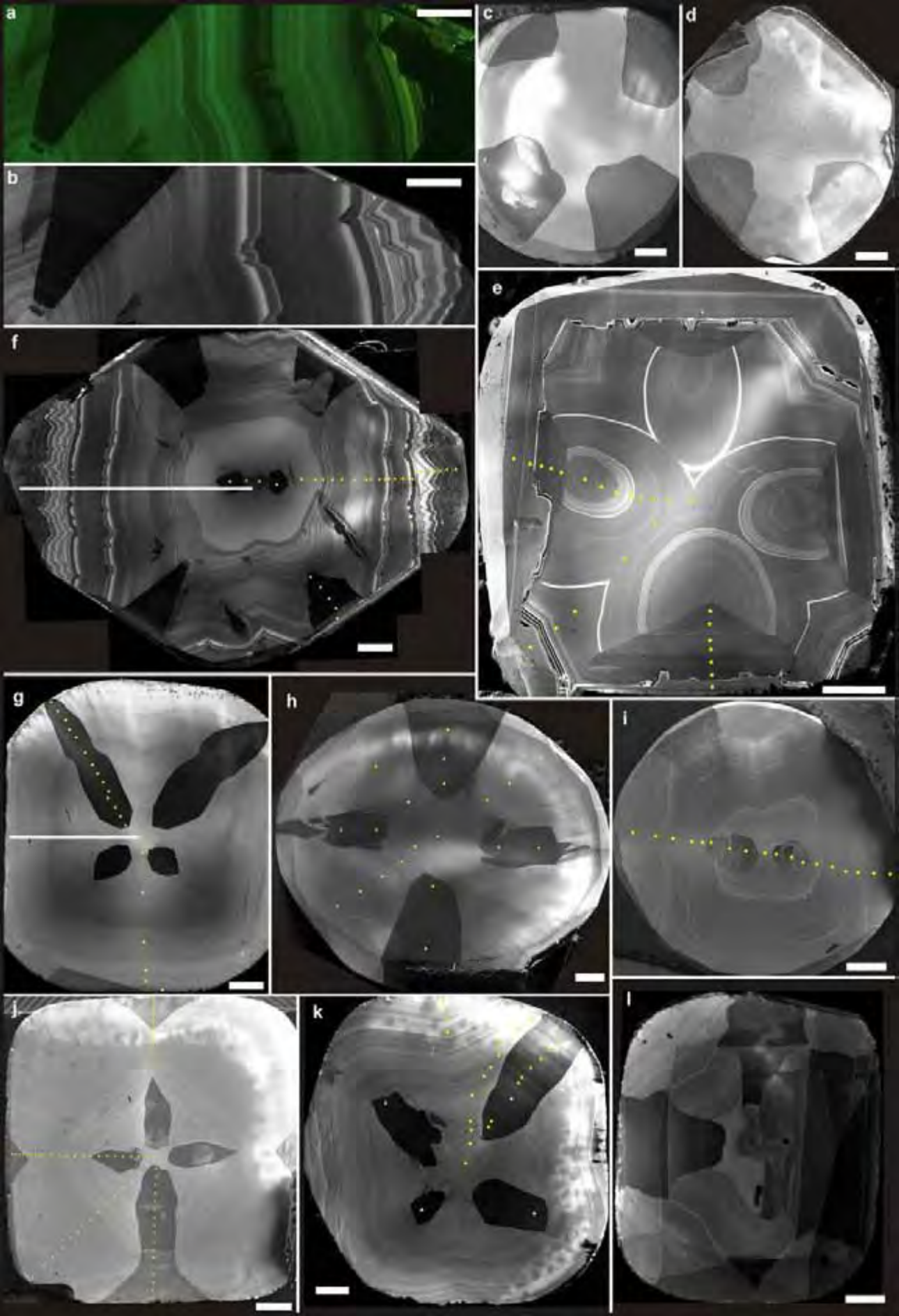
a
b
c
d
e
f
g
h
i
j
k
l

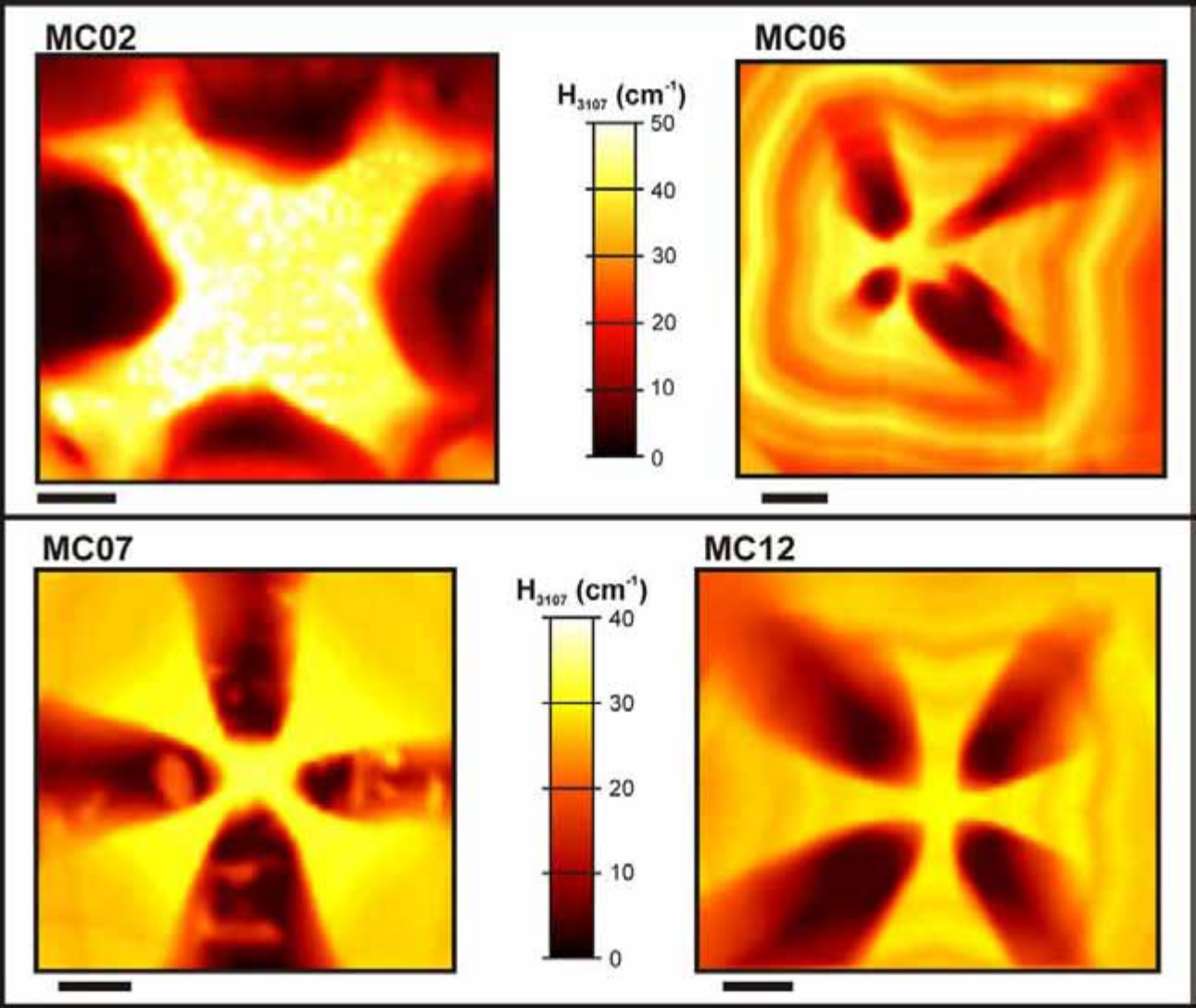
MC02
MC06
H_{3107} (cm^{-1})
50
40
30
20
10
0
MC07
MC12
H_{3107} (cm^{-1})
40
30
20
10
0

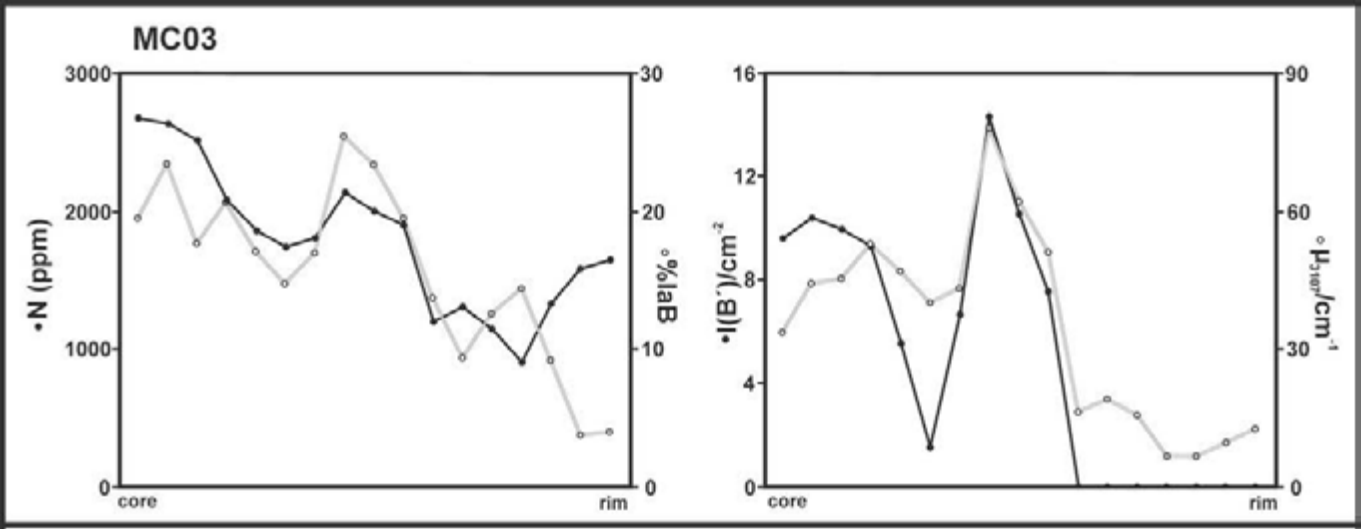
MC03
•N (ppm)
°%laB
•I(B´)/cm-2
°μ193f/cm-1
core
rim

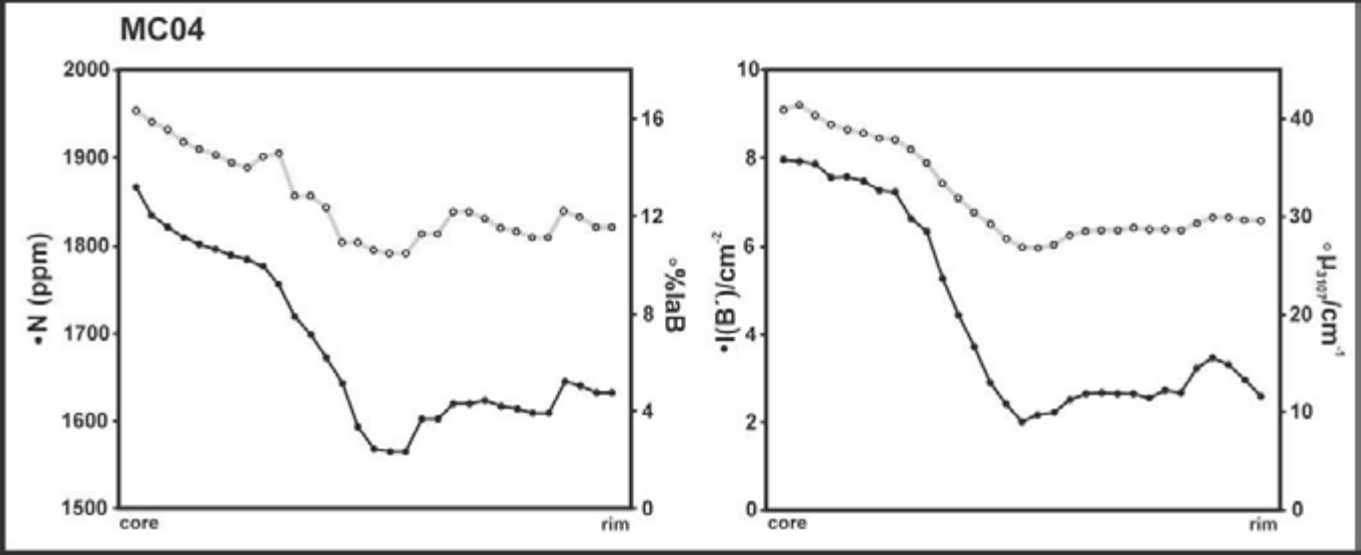
MC04
•N (ppm)
°%laB
•I(B´)/cm-2
°μ193f/cm-1
core
rim

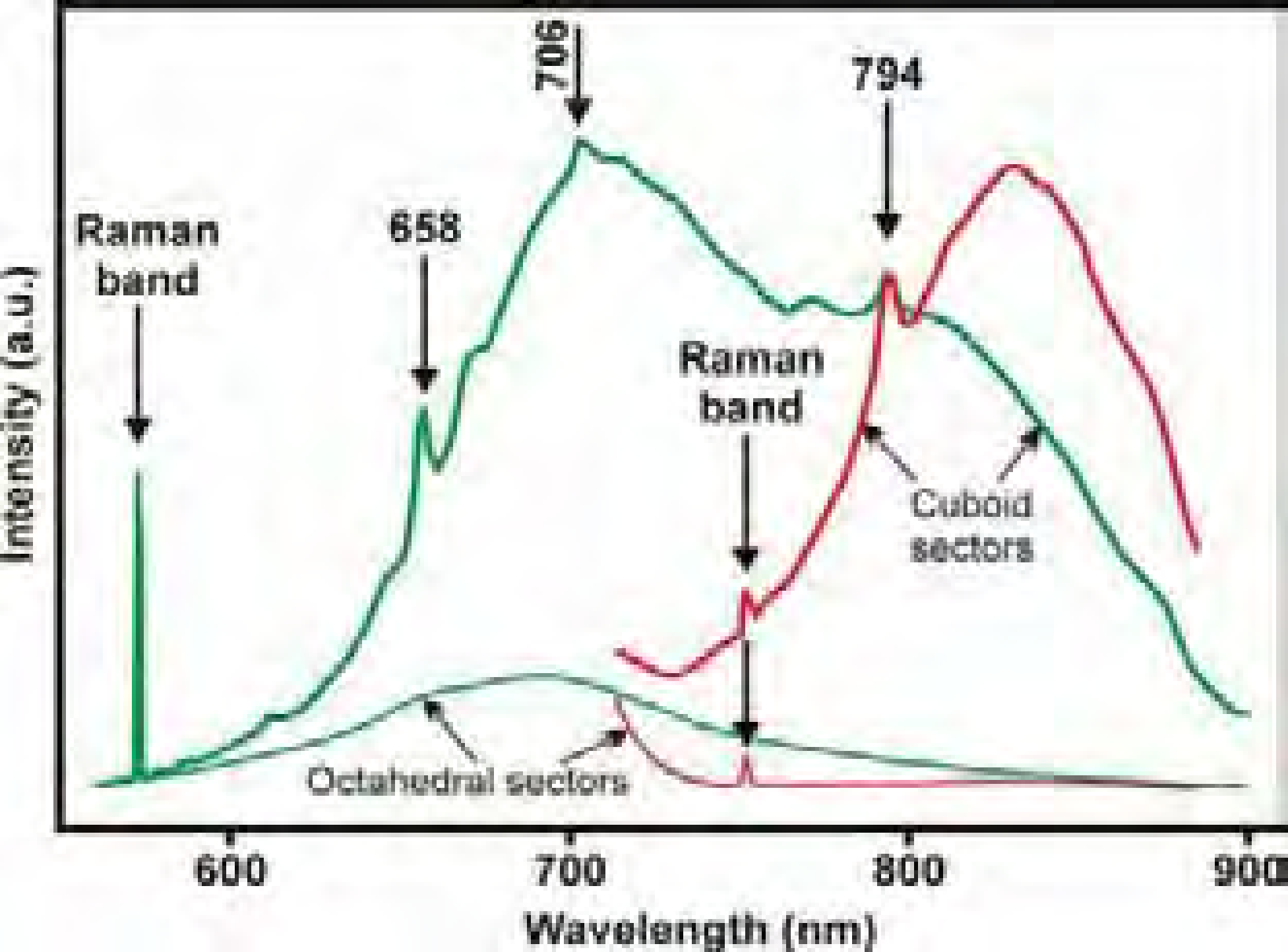
706
794
Raman band
658
Raman band
Cuboid sectors
Octahedral sectors
Intensity (a.u.)
600
700
800
900
Wavelength (nm)

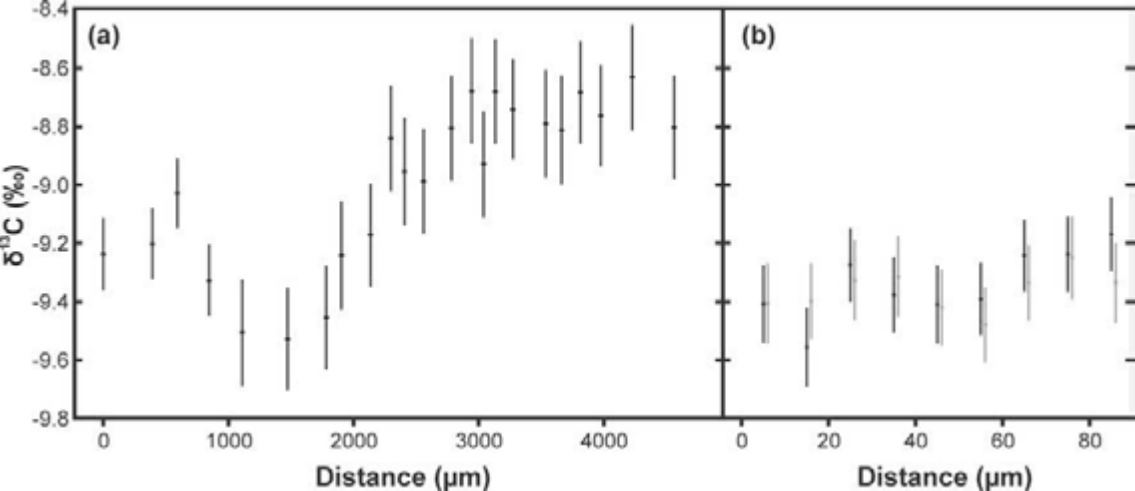
(a)
(b)
δ13C (‰)
-8.4
-8.6
-8.8
-9.0
-9.2
-9.4
-9.6
-9.8
0
1000
2000
3000
4000
Distance (μm)
0
20
40
60
80
Distance (μm)

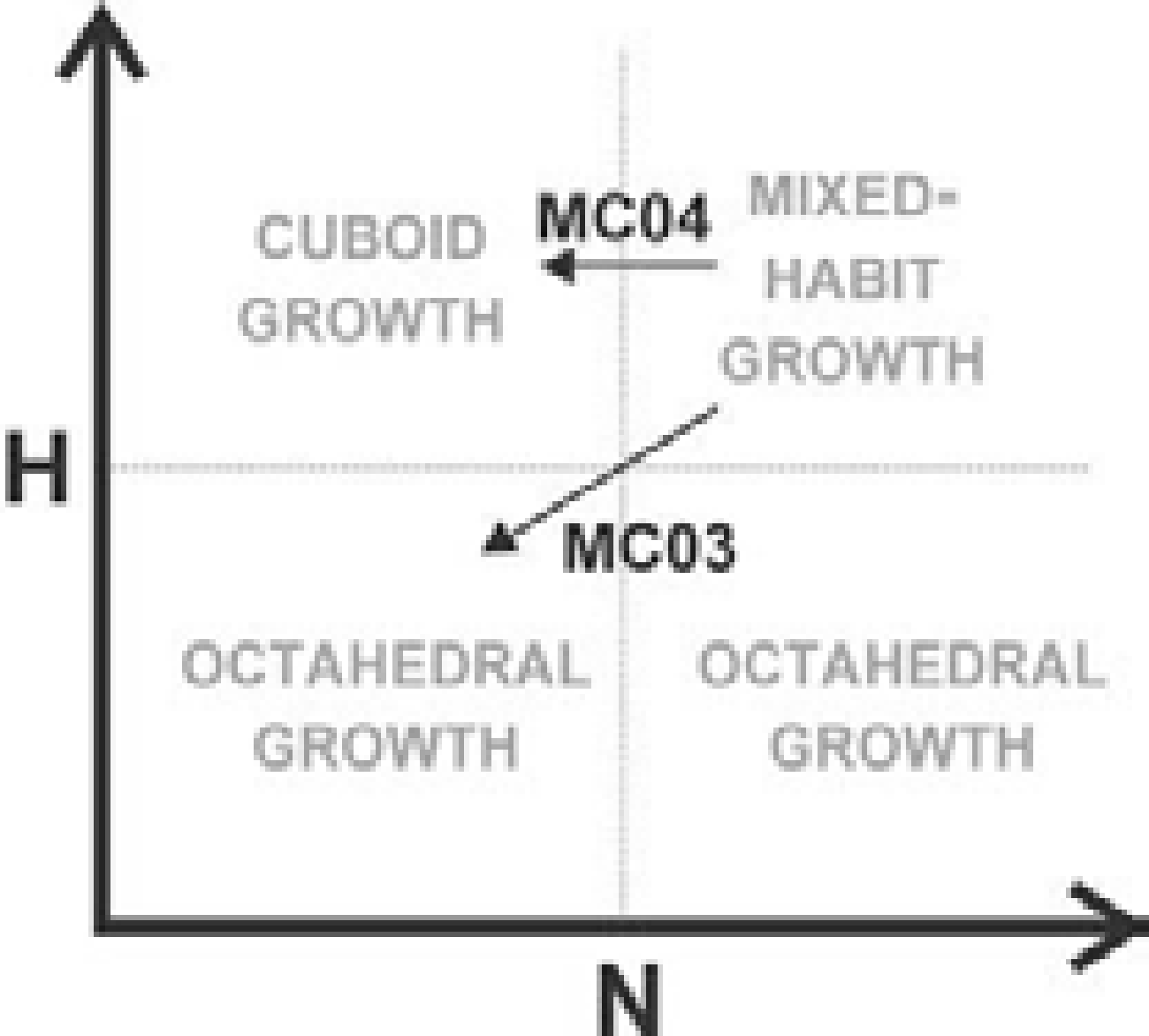
CUBOID GROWTH
MC04
MIXED-HABIT GROWTH
MC03
H
OCTAHEDRAL GROWTH
OCTAHEDRAL GROWTH
N

Sample	Sector	N (ppm)	%IaB (%)	H @ 3107 (cm^{-1})	H @ 1405 (cm^{-1})	B' area (cm^{-2})
MC01	C	1549	10.2	26.3	6.5	6.5
	O	2226	3.4	3.3	0.0	0.0
MC02	C	1500	21.2	67.3	12.8	0.0
	O	2113	23.3	3.9	1.2	196.7
MC03	C	1950	23.4	67.3	15.5	13.1
	C to O	1383	3.2	7.5	1.7	0.0
	O	2715	11.2	11.2	3.2	0.0
MC04	C core	1658	14.6	36.5	9.1	7.3
	C rim	1511	10.1	27.0	6.6	3.0
	O core	2100	8.0	17.5	5.1	1.9
	O rim	1715	8.5	21.0	5.0	2.0
MC05	C core	2050	20.0	77.0	15.6	8.0
	C rim	1480	12.0	39.0	8.6	0.0
	O	2300	13.0	7.0	2.0	
MC06	C	1784	18.9	49.2	12.0	9.5
	O	2335	9.7	8.4	2.6	0.0
MC07	C	1679	15.5	37.8	9.6	0.0
	O	2302	11.7	4.7	0.0	0.0
MC08	C	1866	22.0	52.7	12.8	14.0
	O	2642	5.6	8.8	2.4	0.0
MC09	C	1600	12.2	30.6	7.4	5.2
	O	2250	4.3	7.5	2.0	0.0
MC10	C	1483	10.9	28.4	6.8	0.0
	O	2120	7.0	3.3	0.0	0.0
MC11	C	1575	12.7	31.5	7.5	0.0
	O	2235	7.5	4.1	0.0	0.0
MC12	C	1780	15.7	35.4	9.0	5.3
	O	2335	12.3	4.7	0.0	0.0
MC13	C	1600	12.8	29.9	7.4	0.0
	O	2200	8.1	7.2	2.1	0.0